High Brightness Electron Sources

Richard L. Sheffield, Los Alamos National Laboratory *

ABSTRACT

High energy physics accelerators and free electron lasers put increased demands on the electron beam sources. This paper describes the present research on attaining intense bright electron beams using photoinjectors. Recent results from the experimental programs will be given. The performance advantages and difficulties presently faced by researchers will be discussed, and the following topics will be covered. Progress has been made in photocathode materials, both in lifetime and quantum efficiency. Cesium telluride has demonstrated significantly longer lifetimes than cesium antimonide at 10^{-8} torr. However, the laser system is more difficult because cesium telluride requires quadrupled YLF instead of the doubled YLF required for cesium antimonide. The difficulty in using photoinjectors is primarily the drive laser, in particular the amplitude stability. Finally, emittance measurements of photoinjector systems can be complicated by the non-thermal nature of the electron beam. An example of the difficulty in measuring beam emittance is given.

I. INTRODUCTION

The following two sections of this paper cover the basic photoinjector types and their operational characteristics. The subsequent section covers the measurement of emittance using the quadrupole scan technique. Although the quad scan is a commonly used technique for measuring emittance, in a photoinjector-based system this technique can lead to erroneous emittance measurements.

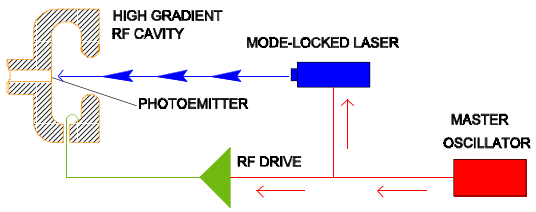

Figure 1 Basic components of a photoinjector are a laser, a photocathode, an rf source, and an rf cavity.

Photoinjectors [1], conceptually shown in Figure 1, have several unique characteristics. A high gradient rf cavity is used to supply the accelerating field. The high-gradient not only reduces space charge effects, but the gradient also enables laminar flow from the cathode through the accelerator to the beamline. Since the electron beam does not undergo transverse or axial mixing, a large fraction of the emittance growth due to space charge can be corrected by a technique called emittance compensation [2]. The high gradient also allows the extraction of high charge for closely spaced pulses resulting in a high average current [3].

Since the electron source is a photocathode illuminated with a laser, the machine designer has complete control over the spatial and temporal characteristics of the electron emission process. The gun can directly produce very short electron pulses limited only by the gun gradient and charge in the pulse. For instance, 1 nC from a cathode with a surface gradient of 30 MV/m will have a 6 ps pulse length.

II. BASIC PHOTOINJECTOR TYPES

The motivation for the first photoinjector experiment, shown in Figure 2, was the need for an electron source that has an rms emittance of less than 40 π mm-mrad and the capability of generating greater than 1 A average current. From the first use of a photoinjector in 1985 [1], many different systems have been designed to meet the needs of very different applications. The applications include high-average-current electron beams, high-brightness source for free-electron lasers and colliders, high pulse charges for wakefield accelerators, high-duty factor picosecond high-energy x-ray pulses, and picosecond soft x-rays by Compton scattering. The advantage of this source for Compton scattering is that the drive laser for the photocathode can be used as the scattering laser. Using the drive laser provides sub-picosecond synchronization of the electron pulse and the laser pulse.

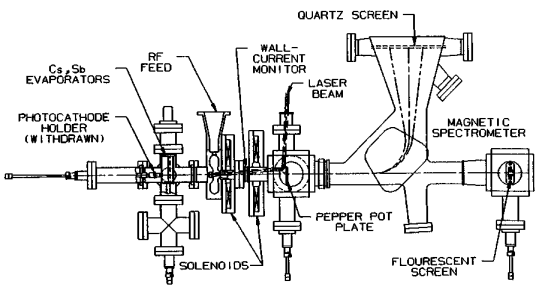

Figure 2 The first photoinjector experiment demonstrated an emittance of less than 30 π mm-mrad at 10 nC, a maximum 27 nC per 53 ps long micropulse, and 2.9 A average current for a 6 μs long macropulse. The current density was estimated to be 600 A/cm^2 from a Cs_3Sb cathode.

Research is still proceeding on high-average current machines at Boeing [4], and at Bruyeres-le-Chatel [5]. The first demonstration of a high-average current using a

* Work supported by Los Alamos National Laboratory Directed Research and Development under the auspices of the United States Department of Energy.

photoinjector was on the Boeing accelerator. This 25% duty factor machine has demonstrated an average current of 32 mA at 5 MeV, giving a average beam power of 160 kW. The macropulse average current was 0.13 A. The beam emittance was 5 to 10 π mm-mrad for 1 to 7 nC pulse charge. An example of the machine located at Bruyeres-le-Chatel is shown in Figure 3.

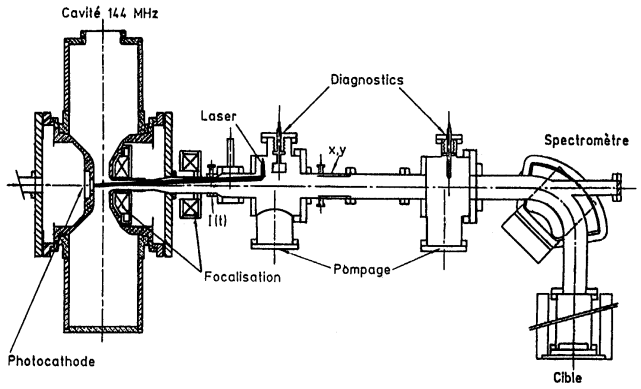

Figure 3 Photoinjector at LEL-HF Bruyeres-le-Chatel. RF cell produces a 2.0 MeV beam at 5 nC with a pulse length of 20 to 50 ps. They have measured 4 π mm-mrad at 1 nC.

Many designs are based on the work done at Brookhaven National Laboratory at 2856 Mhz [6]. A schematic of one of their 1-1/2 cell guns is shown in Figure 4.

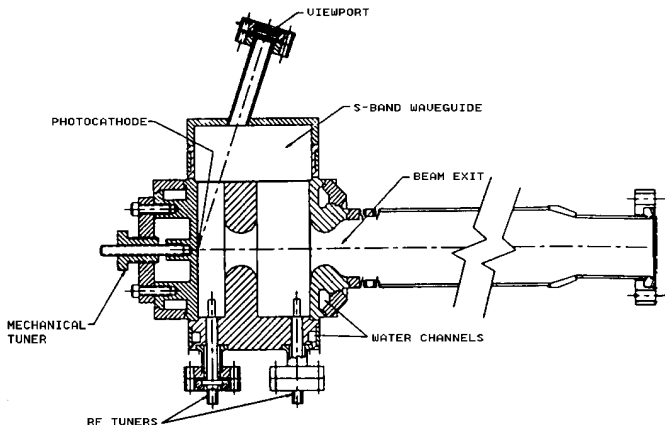

Figure 4 Brookhaven's 2856 MHz photoinjector operates at 3 MeV and has produced 4 π mm-mrad at 1 nC with a cathode field of 70 MV/m. The gun has generated 4.5 MeV beams.

The Brookhaven type of gun is being used for advanced accelerator studies, free-electron lasers, and linear collider injectors. One of the advantages of operating near 3 GHz is the higher cathode surface electric fields that can be obtained relative to operating at lower frequencies.

A new photoinjector operating at 17 GHz has been constructed at the Massachusetts Institute of Technology. This gun has 1-1/2 cells with peak surface fields of 250 MV/m and a peak cathode surface field of 200 MV/m. The rf source is a gyro-amplifier developed at MIT [7].

III. PHOTOINJECTOR OPERATIONAL CHARACTERISTICS

This section covers the operational characteristics of photoinjectors. This section is covers three topics: photocathodes, photocathode lasers, and photoinjector performance.

A. Photocathodes

Photocathodes can be divided into two classes based on quantum efficiency (QE): low QE and high QE.

Low QE cathodes are characterized by having reduced vacuum requirements and are relatively easy to produce. These cathodes fall into two groups, metals and thermionic emitters.

Many different metals have been considered for photoinjector cathodes. Copper and magnesium [8] are the most common choices. Other metals that have been considered are: Al, Au, stainless steel, Sm, Y, W, Zn, Au, Mo, Ta, Pd, Zr, Ba, Na, Ca [9],[10]. Measurements of quantum efficiency vary considerably among individual researchers. This variation can in part be attributed to differences in samples, preparation techniques, and contamination before and during measurements. Also the UCLA group has reported non-uniform emission occurring after use in a photoinjector [11]. Overall, the measured quantum efficiency of metals varies from less than 10^{-8} to 3 x 10^{-3} near a wavelength of 250 nm.

The thermionic emitters, LaB_6 [12] and BaO, have also been used as cathodes, both heated and unheated. Again, the measured quantum efficiencies are dependent on many factors and varies among laboratories. Quantum efficiencies of greater than 10^{-4} have been measured. The temporal response in the picosecond regime for these cathodes has not been measured.

Another metal cathode being used in the ATF at the Kharkov Institute is pressed BaNi. They quote a QE of 1.7 x 10^{-3} [13].

High QE photocathodes, in general, require a good vacuum and have a more sophisticated fabrication procedure. These types of cathodes can be subdivided into three categories: multialkali, crystal-like, and GaAs.

The Cs_3Sb multialkali cathode was the first cathode used in a photoinjector. Since then a large number of other multialkali cathodes have been used, such as CsK_2Sb, AgO:Cs, CsNaKSb, K_3Sb, and NaK_2Sb.

Multialkali cathodes have a significant advantage over metal cathodes. These cathodes have QE's over 2% at 532

nm, making the drive laser requirements less stringent. Unfortunately, since they are used with lower energy photons, they tend to be very susceptible to contamination and require 10^{-10} torr vacuum systems. Because of contamination issues, these cathodes have limited lifetimes.

The crystal-like cathodes, Cs_2Te, CsI, K_2Te all require laser wavelengths of at least 250 nm for quantum efficiencies over 2%. Their advantage is that they can survive in 10^{-8} vacuum systems [9],[14]. Also these cathodes can be rejuvenated by heated to 150 C and reused.

Finally, GaAs has been used for many years as a polarized electron source. KEK plans to use this cathode in a specially cleaned photoinjector that exhibits almost no change in impurities and background pressure with and without rf power [15].

There is a wide variety of photocathodes to choose from based on the system requirements. The photocathode, though difficult, is no longer a major impediment to using this technology.

B. Photoinjector Lasers

The key to the stability and reliability of a photoinjector is the drive laser. The advantage of using a laser is that the cathode can be illuminated with any temporal and spatial profile required to optimize the gun performance. Lasers have excellent temporal stability, with almost all of the present systems in use having less than picosecond temporal jitter. Also, if only single pulses are required, a laser can generate very large energy per pulse (LLNL NOVA laser can generate nearly 1 kJ in less than 10 ns).

The remaining difficulty in the laser systems is the macropulse to macropulse amplitude stability. Achieving less than 10% amplitude stability is very difficult with present systems. The technology exists to achieve less than 1% stability, but not the resources.

Lasers can generate high peak energy in short pulses easier than long (many microseconds) pulses. It follows that for long pulse trains a minimum QE of 0.5% is required.

One other issue that can be critical to stable operation is pointing stability. Since the laser defines the spatial profile of the emission, the laser must be stably pointed at the cathode. For example, the large solenoid around the gun region of the Advanced Free-Electron Laser [16] acts to amplify small transverse spatial variations of the cathode position. This amplification occurs because of the long distance from the large solenoid to the first focusing element (2.5 m lever arm). Even though the cathode diameter is 8 mm, a shift of 100 microns in the centroid will image to a 25 micron shift in the middle of the wiggler.

C. Performance Characteristics

Photoinjectors routinely generate greater than 500 A/cm^2. For most systems this current density is limited only by the field gradient on the cathode or the laser intensity.

Most photoinjectors generate between 1 and 10 nC per micropulse. Argonne National Lab has generated greater than 50 nC per micropulse.

Electron pulse lengths are limited by space charge effects in the first few centimeters in front of the cathode. Typically, less than 10 ps pulses are generated for 1 nC of charge in a micropulse (in the AFEL 6 ps for 1 nC)

The measured electron beam's rms emittance varies, depending on the machine design, between 1 and 5 π mm-mrad for 1 nC in a micropulse. Some newer designs give less than 1 π mm-mrad for 1 nC [17].

IV. EMITTANCE MEASUREMENTS ON A PHOTOINJECTOR

Emittance measurements in a photoinjector are complicated by one of the photoinjector's advantages. Because of the rapid acceleration and lack of other beamline components in the gun region, the longitudinal phase space of the beam does not thermalize. As a result of the non-thermalization, different longitudinal parts of the beam propagate with their own trajectories. This complicates the analysis of the beam's phase space ellipse. Commonly used techniques for measuring emittance, such as pepperpot technique or quadrupole scans, can lead to erroneous emittance and phase-space ellipse measurements.

In the first photoinjector experiment, a pepperpot was used to measure the emittance [18]. Because of the longitudinal variations in phase-space, the emittance was underestimated by a factor of four. In this section, I will describe difficulties in using a quadrupole scan technique to determine the beam's emittance.

For a thin lens, the rms unnormalized emittance, ε_{un} can be calculated by fitting the beam spot size x_s to the coefficients of $1/f$ in the following

$$x_s^2 = x_{\min}^2\left[1+\{L^2\varepsilon_{un}(1-f_w/f)/(x_{\min}^2 f_w)\}^2\right],$$

where ε_{un} is the unnormalized rms emittance, L is the spacing between the quadrupole and the image screen, f is the focal length of the quadrupole, f_w is the focal length that gives the minimum spot size x_{min} [19]. The focal length of a quadrupole is $\beta\gamma m_e c/(leB)$, where β, γ are the relativistic factors, m_e is the mass of an electron, c is the speed of light, l is the quadrupole length, e is the electron charge, and B is the quadrupole field gradient.

For a thick lens, the spot size x_s can be fit using the Twiss parameters 20 with the following formula,

$$x_s^2 = \varepsilon_{un}\left[m_{12}^2\gamma_q - 2m_{11}m_{12}\alpha_q + m_{11}^2\beta_q\right],$$

where γ_q, β_q, and α_q are the Twiss parameters of the beam at the quadrupole. The coefficients of the Twiss parameters are from the Twiss parameter transfer matrix for a thick lens,

$$m_{11} = \cos(\theta) - d\theta \sin(\theta)/L$$
$$m_{12} = d\cos(\theta) + L\sin(\theta)/\theta$$
$$\theta = L\sqrt{eB/(\beta\gamma mc)}$$

where d is the quadrupole's axial length and L is the spacing from the end of the quadrupole to the image screen. Using the identity $\beta_q\gamma_q-\alpha_q^2=1$, then the rms unnormalized emittance can be calculated from the coefficients of the fit.

The experimental data and the fit using the Twiss parameters are shown in Figure 5. The thin lens fitting procedure was also used on the experimental data and the results were within 10%. The rms emittance as calculated from the fit for either the data spot sizes or for the PARMELA spot sizes is 2.3 π mm-mrad. The PARMELA simulation gives an integrated rms emittance of 5 π mm-mrad.

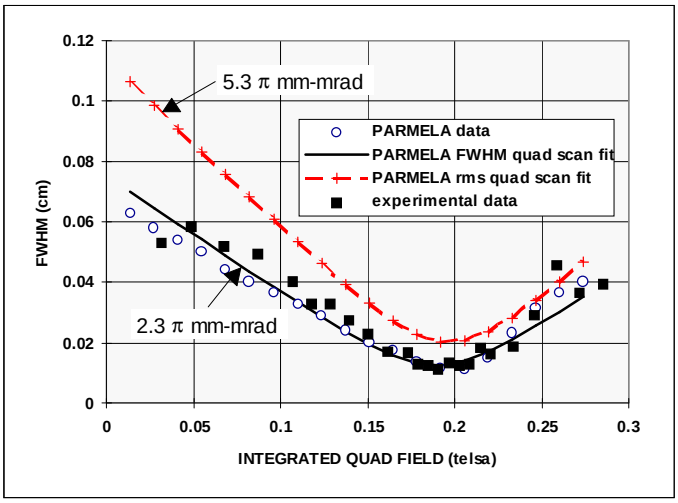

Figure 5 The data and PARMELA simulation are for a quadrupole scan with the FWHM taken at a screen 30 cm downstream from the quadrupole. The electron pulse is 1.9 nC at 17.2 MeV. The beam is produced by a Cs_2Te cathode illuminated by a 8 ps laser pulse. The laser's spatial profile is a 6 mm FWHM gaussian clipped with a circle of 5.2 mm diameter. The FWHM of each slice at the screen is plotted as a function of the quadrupole gradient.

The discrepancy in emittance is due to the manner in which the data is analyzed. Measuring the full distribution of an image on a screen is susceptible to many errors. In particular, the correction of data due to baseline shifts and the non-linear response of cameras, especially at low intensity, is very difficult. Unfortunately, the rms emittance numbers are very sensitive to the tails of the distribution. So instead, many researchers measure an unambiguous parameter of the spot-size, the full-width half-maximum. As can be seen in Figure 5, the agreement between the FWHM's from the experimental measurement and the FWHM's from PARMELA is very good. However, because of the longitudinal dynamics of different slices, the FWHM measurement cannot be used to directly compute the beam's emittance. In Figure 5, the dashed curve shows the FWHM as calculated from the rms spot sizes from PARMELA. Now the quadrupole scan fit gives an emittance close to the calculated emittance.

The variation of FWHMs at the screen of the individual slices with changing quadrupole strength is shown in Figure 6. The reason for the discrepancy in emittance is readily apparent. The ends of the micropulse are focused differently than the middle of the pulse. The FWHM spot size measurement is thus complicated by the different longitudinal portions of the pulse contributing to the FWHM in differing amounts as the quadrupole is varied.

The minimum spot size is dependent on the cathode temperature and any residual magnetic field on the cathode. Thus far, the cathode temperature of Cs_2Te has not been measured. The cathode initial emittance can be inferred by adding a minimum spot size to the PARMELA spot sizes (square root of sum of squares). From the experimental data, this gives an initial emittance of 2.8 π mm-mrad, corresponding to a transverse energy of 1.2 eV. The partition of this energy between residual magnetic field at the surface of the cathode and cathode temperature cannot be determined.

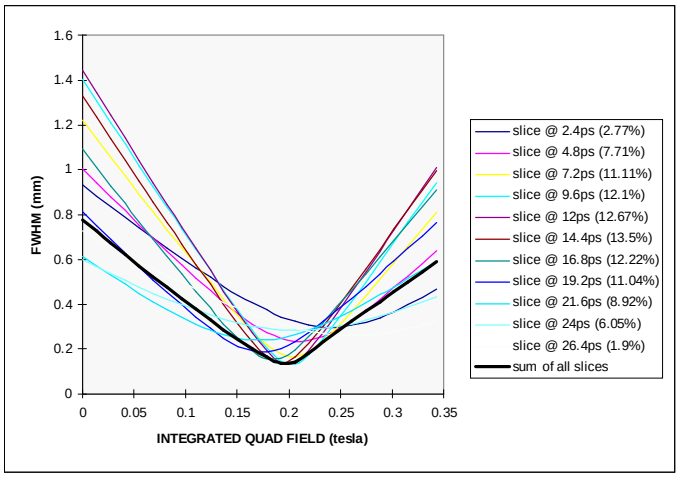

Figure 6 The TAPE2 PARMELA output was processed by dividing the longitudinal length of the pulse into 11 equal segments. The FWHM of each slice at the screen is then plotted as a function of the quadrupole gradient. The fraction of charge in each slice is shown in the legend. The thick black line is the summation of all the individual FWHM's. To make sure the slicing was done properly, the summation is compared with the normal output of PARMELA (an integration over all slices).

Finally, the large solenoid around the cathode region is the main steering and focusing element in the system. This

results in the beam's phase space ellipse being very sensitive to the magnitude of the solenoid's field. In the case shown above, the measured value of the large solenoid's field was within 1% (the experimental error was 5%) of the value predicted by PARMELA. Changes in magnetic field as small as 1% are easily observable in simulation and have a significant effect on the beam's Twiss parameters.

V. SUMMARY

Photoinjector technology has had significant developments in the decade since its inception. Designs now span a large range in frequencies and electron pulse requirements. The photocathode source, though difficult, is not a major impediment to implementing a photoinjector-based system. However, the amplitude stability of the drive laser for the photocathode is an issue.

The measurement of the phase space of the pulse produced from a photoinjector is not straightforward. An exact comparison with simulation is required for a thorough understanding of the phase space of the pulse. For a good simulation, an accurate measurement of magnetic fields, photocathode laser profile, accelerating fields, and phasing of the laser and rf is required. With accurate measurements, good agreement between experiment and simulation can be obtained.

A large solenoid around the cathode region is sometimes used to reduce the emittance of the beam by the technique of emittance compensation. In these types of photoinjectors, the transport of the beam downstream is very sensitive to the location of the electron emission, collinearity of the magnetic field with the beam trajectory, and the magnitude of the magnetic field.

The author is indebted to many individuals for information on their projects. In particular, I wish to thank Chris Travier, Steve Kong, John Adamski, Shien-Chi Chen, Harold Kirk, Claudio Pelligrini, and Jim Simpson.

[1] J. S. Fraser, R. L. Sheffield, and E. R. Gray, "High-Brightness Photoemitter Development for Electron Accelerator Injectors," *Laser Acceleration of Particles AIP Conf. Proc.*, no. 130, pp. 598, 1985; J. S. Fraser, R. L. Sheffield, and E. R. Gray, "A New High-Brightness Electron Injector for Free Electron Lasers," *Nucl. Inst. And Methods*, vol. 250, pp. 71-76, 1986.

[2] B. E. Carlsten, *Nucl. Inst. And Methods*, vol. A285, pp 313-319, 1988.

[3] J. S. Fraser and R. L. Sheffield, *IEEE J. Quant. Elec.*, vol. QE-23, pp. 1489-1496, 1987.

[4] D. H. Dowell, K. J. Davis, K. D. Fridell, E. L. Tyson, C. A. Lancaster, L. Milliman, R. E. Rodenburg, T. Aas, M. Bemes, S. Z. Bethel, P. E. Johnson, K. Murphy, C. Whelen, G. E. Busch, and K. K. Remelius, "First Operation of a Photocathode Radio Frequency Gun Injector at High Duty Factor," *Appl. Phys. Lett.*, vol. 63, no. 15, pp. 2035-2037, (1993).

[5] S. Joly et al., "Progress Report on the BRC Photoinjector," *Proc. 1990 European Part. Accel. Conf.*, Nice June 12-16, pp. 140-142, 1990.

[6] K. Batchelor, et al. "Performance of the Brookhaven Photocathode RF Gun," *Nucl. Inst. and Methods*, vol. 318, pp. 372-376, 1992.

[7] S. C. Chen, J. Gonichon, L. C-L. Lin, R. J. Temkin, S. Trotz, B. G. Danly, and J. S. Wurtele, "High Gradient Acceleration in a 17 Ghz Photocathode RF Gun," *Proc. 1993 Par. Accel. Conf.*, vol. 4, pp. 2575-2577, 1993.

[8] J. Fischer, T. Srinivasan-Rao, and T. Tsang, "Mg Photocathode Performance Overview," *Sources '94, Schwerin, Germany, Sept. 29 - Oct.4*, pp.287-289, 1993.

[9] G. Suberlucq, "Photocathodes for the CERN CLIC Test Facility," *Sources '94, Schwerin, Germany, Sept. 29 - Oct.4*, pp.557-561, 1993; C. Travier, "High-Brightness Photocathode Electron Sources," *6th Workshop on Advanced Accel. Concepts, Lake Geneva, WI, June 12-18*, 1994.

[10] Private communication from M. E. Conde, UCLA/ANL.

[11] Private communication from C. Pellgrini, UCLA.

[12] D. J. Bamford, M. H. Bakshi, and K. A. G. Deacon, "The Search for Rugged, Efficient Photocathode Materials," *Nucl. Inst. And Methods*, vol. A318, pp. 377-380, 1992.

[13] Y. Tur, "A Photoinjector Test Accelerator Complex: Current Status and Future Prospects," *Sources '94, Schwerin, Germany, Sept. 29 - Oct.4*, pp.572-576, 1993.

[14] S. H. Kong, J. Kinross-Wright, D. C. Nguyen, and R. L Sheffield, "Cesium Telluride Photocathodes," *J. Appl. Phys.*, vol. 77, no. 11, pp 1-8, 1995.

[15] M. Yoshioka, "High Gradient Study on UHV Copper Cavity at S-Band," *Sources '94, Schwerin, Germany, Sept. 29 - Oct.4*, pp.624-629, 1993.

[16] R. L. Sheffield, R. H. Austin, K. D. C. Chan, S. M. Gierman, J. M. Kinross-Wright, S. H. Kong, D. C. Nguyen, S. J. Russell, and C. A. Timmer, "Operation of the High Brightness LINAC for the Advanced Free-Electron Laser Initiative at Los Alamos," *Proc. 1993 Par. Accel. Conf.*, vol. 4, pp. 2970-2972, 1993.

[17] H. Kirk, "A Comparison of L-Band and C-Band RF guns as Sources for Inline-Injection Systems," *Sources '94, Schwerin, Germany, Sept. 29 - Oct.4*, pp.392-398, 1993.

[18] J. S. Fraser, R. L. Sheffield, E. R. Gray, and P. M. Giles, R. W. Springer, and V. A. Loebs, "Photocathodes in Accelerator Applications," *1987 IEEE Part. Accel. Conf, March 16-19, Washington, D. C.*, pp. 1705-1709, 1987; R. L. Sheffield, "Photocathode RF Guns," *AIP Conf. Proc.*, vol. 2, no. 184, pp. 1500-1531, 1989.

[19] B. E. Carlsten, J. C. Goldstein, P. G. O'Shea, and E. J. Pitcher, "Measuring Emittance of Nonthermalized Electron Beams," *Nucl. Inst. And Methods*, vol. A331, pp. 791-796, 1993.

[20] S. Humphries, Jr., "Charged Particle Beams," *John Wiley and Sons, Inc.*, pp. 143, 1990.